Simulation of ENSO Related Surface Wind Anomalies with an Atmospheric GCM Forced by Observed SST

MOJIB LATIF, JOACHIM BIERCAMP AND HANS VON STORCH

Max-Planck-Institut für Meteorologie, Hamburg, Federal Republic of Germany

MICHAEL J. MCPHADEN

NOAA/Pacific Marine Environmental Laboratory, Seattle, Washington

EDILBERT KIRK

Meteorologisches Institut der Universität, Hamburg, Federal Republic of Germany

(Manuscript received 2 June 1989, in final form 2 November 1989)

ABSTRACT

The ECMWF-T21 atmospheric GCM is forced by observed near-global SST from January 1970 to December 1985. Its response in low level winds and surface wind stress over the Pacific Ocean is compared with various observations.

The time dependent SST clearly induces a Southern Oscillation (SO) in the model run which is apparent in the time series of all variables considered. The phase of the GCM SO is as observed, but its low frequency variance is too weak and is mainly confined to the western Pacific.

Because of the GCM's use as the atmospheric component in a coupled ocean–atmosphere model, the response of an equatorial oceanic primitive equation model to both the modeled and observed wind stress is examined. The ocean model responds to the full observed wind stress forcing in a manner almost identical to that when it is forced by the first two low frequency EOFs of the observations only. These first two EOFs describe a regular eastward propagation of the SO signal from the western Pacific to the central Pacific within about a year. The ocean model's response to the modeled wind stress is too weak and similar to the response when the observed forcing is truncated to the first EOF only. In other words, the observed SO appears as a sequence of propagating patterns but the simulated SO as a standing oscillation.

The nature of the deviation of the simulated wind stress from observations is analyzed by means of Model Output Statistics (MOS). It is shown that a MOS-corrected simulated wind stress, if used to force an ocean GCM, leads to a significant enhancement of low frequency SST variance, which is most pronounced in the western Pacific.

1. Introduction

In this paper we consider the ability of an atmospheric general circulation model (AGCM) to reproduce observed tropical low frequency anomalies. The reason for doing this is that the model, which is the T21 version of the ECMWF (European Centre for Medium Range Weather Forecasts) GCM, is used as the atmospheric component in a coupled GCM of the tropical Pacific Ocean (Latif 1987) and the global atmosphere. The coupled GCM has been used to study the effect of strong westerly wind bursts over the western Pacific (Latif et al. 1988a). In another experiment we found the coupled GCM unable to generate self-excited low frequency variability (Latif et al. 1988b). The reasons for the model's failure were not quite clear, and we speculated that the atmospheric component might be blamed for part of the failure.

GCM data are also used to improve operational wind field analyses by blending observed winds with nowcasted winds (Leetma and Ji 1989). Consequently, it is of interest to compare the T21 simulated winds with observations, and to examine the sensitivity of the ocean circulation to deviations between these datasets.

Recently a multiyear simulation was performed with the ECMWF atmospheric GCM in its T21 resolution using observed SST changes during the period January 1970 to December 1985 to force the model. Here we investigate the tropical response of the T21 model to these time dependent SST anomalies, which include several cold and warm events, and compare the model data with observations which were available to us.

Similar experiments have been conducted at other institutions: Lau (1985) performed two 15-year inte-

Corresponding author address: Dr. Mojib Latif, Max Planck Institut für Meteorologie, Bundesstrasse 55, D-2000 Hamburg 20, Federal Republic of Germany.

grations with the atmospheric GCM developed at the Geophysical Fluid Dynamics Laboratory (GFDL) using observed month-to-month SST during the period 1962 to 1976 as a lower boundary condition over the tropical Pacific. He shows that the model's circulation in the tropics responds in a realistic way to SST changes during El Niño events. Graham et al. (1988) report on the response of the National Center for Atmospheric Research (NCAR) GCM to prescribed SST anomalies for the period 1961 to 1972 (Chervin 1988) in terms of tropical Pacific wind stress. They find that the spatial configuration of the simulated wind stress resembles the observed one, but with less agreement in the non-equatorial regions, and also the amplitude of the model response is too weak.

In this contribution we verify our simulated low level winds and surface wind stresses quantitatively by comparing them to observational data from various sources. These data are described in detail in section 2.

In section 3 we compare time series of surface winds at individual buoy locations, the 850 hPa zonal wind variance along the equator, and the dominant low frequency EOFs of zonal wind stress anomalies over the tropical Pacific.

After having found systematic differences between the simulated and observed surface wind fields, we deal in section 4 with the sensitivity of an ocean GCM to these systematic errors in the wind field. For this purpose a tropical Pacific Ocean primitive equation model has been integrated using the observed and the simulated wind stresses as forcings.

In section 5 we test whether the "Model Output Statistic" (MOS) approach used in numerical weather prediction is successful in overcoming the aforementioned systematic errors.

The paper concludes with a discussion of the results in section 6.

2. Data

a. *Model data*

The model data are obtained from a 16-year integration with the T21 version of the AGCM of the ECMWF (Fischer 1987; Storch 1988). The SST has been specified according to *Climate Analysis Center*-analyses of 40°S–60°N (January 1970 to December 1980) and global (January 1981 to December 1985) SST (Reynolds 1988). Over land, temperature and moisture have been calculated prognostically using prescribed deep soil temperature and moisture. The distribution and surface temperature of sea and land ice have been prescribed climatologically. The initial conditions are taken from 1 January, year 2 of a control run with climatological SST. The model output is stored as monthly means, which are indexed by the date of the SST anomaly. Here we use surface wind stress, 10 m wind, and 850 hPa wind.

b. *Verification data*

Besides the sea level pressure difference between the stations at Darwin and Tahiti, defining a Southern Oscillation Index (SOI), we use the data described below.

1) SURFACE WIND (BUOY DATA)

In situ observations from equatorial buoys (McPhaden and Taft 1988) at 110°W (March 1980; August 1980–December 1982; November 1983–November 1984; May 1985–October 1987), at 124°W (November 1983–October 1984; May 1985–September 1985) and 140°W (May 1984–July 1985; October 1985–September 1987) are available at a level of 4 m. Assuming neutral stability, which is reasonable over the cold eastern Pacific surface water, we approximate the 10 m wind by multiplying the measurements by a factor of 1.1 (Large and Pond 1981).

It should be noted that the monthly buoy wind data are based on two types of vector average measurements. Most are made from a cup and vane anemometer (15-minute averaging interval) and some are made from a propeller and vane anemometer (2-hour averages). Individual 2-hour averages in the zonal and in the meridional component determined from these instruments are consistent with one another to within 0.5 m s^{-1} based on a 4-month experiment on the equator at 140°W (Freitag et al. 1989). The mean differences were 0.09 m s^{-1} in the zonal component (propeller larger) and 0.15 m s^{-1} in the meridional component (cup larger).

These in situ measurements are regarded as being trustworthy, but the time series of wind components are only available at a few locations and are rather short with respect to the typical ENSO time scale of about 3 to 4 years.

2) SURFACE WIND (ANALYSES)

Monthly mean 10 m wind components on a 2° × 2° grid for the period 1950 to 1979 are available from COADS [Comprehensive Ocean–Atmosphere Data Set; for references see Wright (1988)]. COADS is based largely on ship observations, and only little spatial and temporal averaging has entered the final dataset. Along the equator the data are very sparse, but we believe that sufficient data are available to estimate the mean annual cycles shown later in Fig. 2.

For 1980 to 1986, COADS "interim" data recently became available. Because there are only very few observations available on the equator, monthly anomalies have been calculated as area averages over 4° (latitude) by 10° (longitude) grid boxes (Figs. 3, 4 and 5). The accuracy of the anomalies is questionable because of the sparseness of observations in areas with strong horizontal gradients.

3) 850 HPA ZONAL WIND

NMC (National Meteorological Center) analyses of equatorial 850 hPa zonal wind are available from May 1974 to February 1985 (Arkin 1982; Trenberth and Olsen 1988). Note that the wind data are not really "observed" but the output of the NMC operational global data assimilation system, which depends heavily on a forecast model in this data sparse region.

4) PSEUDO-WIND STRESS

FSU (Florida State University) analyses of pseudo-wind stress fields ($|v| \cdot v$) (Goldenberg and O'Brien 1981; Legler and O'Brien 1984) have been obtained from subjective analyses of ship wind observations over the tropical Pacific. The dataset consists of monthly mean pseudostresses for the period 1961 to 1985. The resolution is $2° \times 2°$, and the analyzed area extends from 29°N to 29°S and from 124°E to 70°W. As described by Goldenberg and O'Brien (1981) there was poor data coverage on and south of the equator, so that the analyses are of limited reliability in these data sparse regions. To obtain wind stresses the data were multiplied by $\rho \cdot c_d$, where $\rho = 1.2$ kg m^{-3} is the density of air and $c_d = 1.5 \cdot 10^{-3}$ the drag coefficient.

3. Results

It should be noted that the GCM results shown in this section represent area averages over a grid box of $5.6° \times 5.6°$. Therefore, problems may arise in defining a "local" response, and the verification of the GCM winds may suffer from the low resolution.

a. The Southern Oscillation Index (SOI)

As a measure of the state of the Southern Oscillation we use the sea level pressure difference between Darwin and Tahiti. The observed and simulated time series (Fig. 1) are not well related to each other on time scales of a few months, but on time scales longer than a year the signs of the simulated and observed SOIs do coincide. Cross spectral analysis (not shown) reveals that the variances of the two time series are similar on time scales shorter than one year, but that the coherence is low. On time scales longer than two years, the GCM generated variance is systematically lower than observed. The coherence, however, is large (80% and more) and highly significant (risk < 1%) at these time scales, and the phase spectrum is close to zero. We conclude from these results that the timing of the simulated low frequency changes in the Southern Oscillation is adequately reproduced, but that the intensity of the modeled Southern Oscillation is too weak.

b. Surface winds: annual cycle

First, we compare the simulated surface winds at three locations on the equator (110°W, 124°W, and 140°W) to in situ observations from equatorial buoys (dataset A). As an additional reference COADS (dataset B) is used.

At 124°W there are too few buoys to define a mean annual cycle, but at 110°W and 140°W there are sufficient buoy data available to do so (two months have only 2 samples, otherwise there are at least 3 samples per calendar month). The observed and simulated annual cycles of the zonal and meridional wind component at these two locations are shown in Fig. 2. The

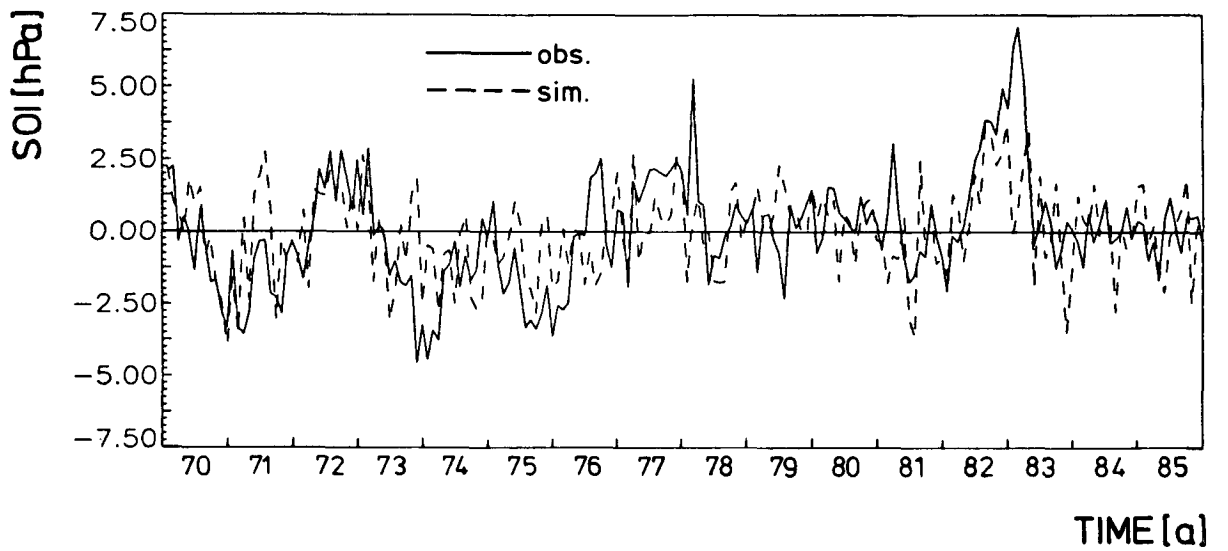

FIG. 1. Simulated (dashes) and observed (solid) Southern Oscillation Index defined by the monthly mean difference of sea level pressure anomalies at Darwin and Tahiti.

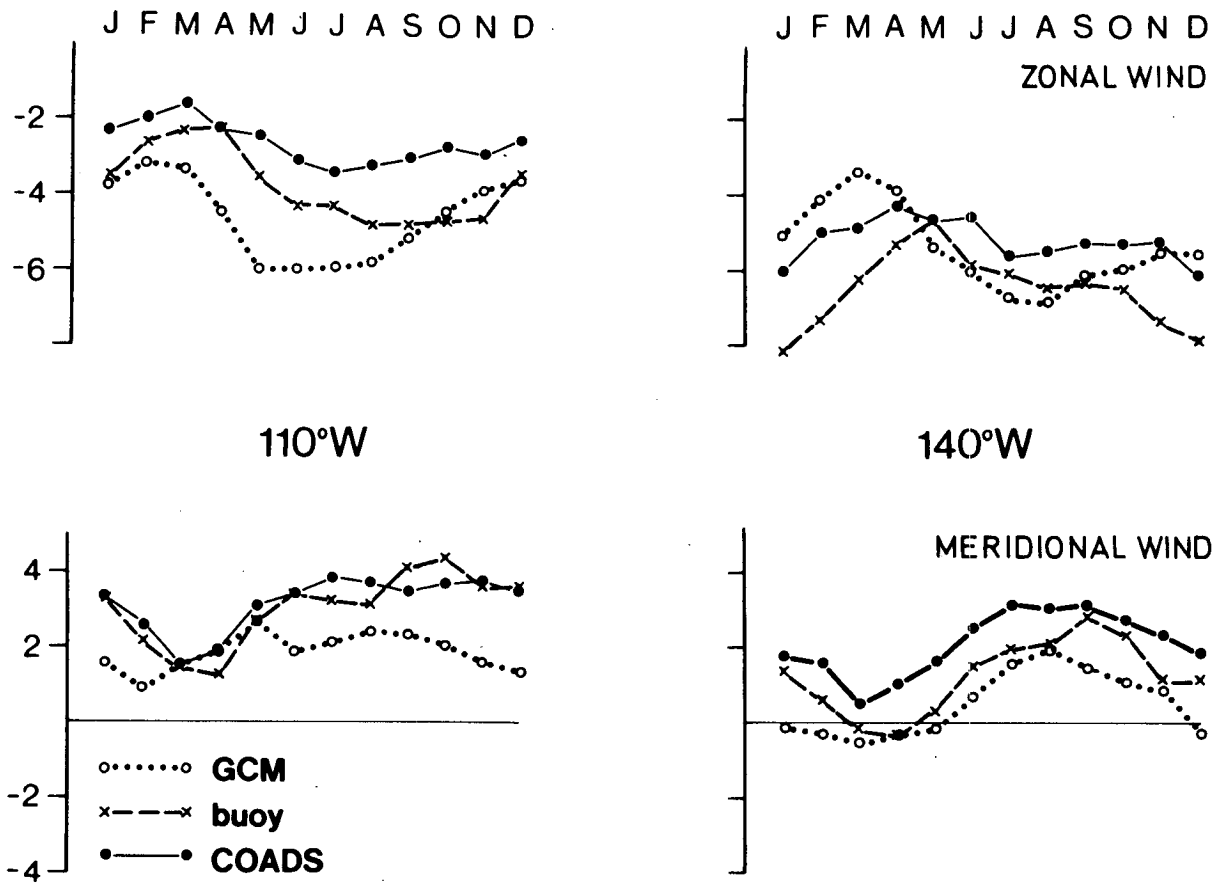

FIG. 2. Mean annual cycles of zonal (top row) and meridional (bottom row) 10 m wind at 110°W (left column) and at 140°W (right column). Units: m s^{-1}. Crosses: buoy data; the raw data were taken at 4 m, from which an estimate of the 10 m wind was obtained by multiplication by 1.1. Solid circles: calculated from January 1950–December 1979 COADS. Open circles: GCM data; a time–area mean from 2.8°S–2.8°N and January 1970 to December 1985 is shown.

COADS annual cycle has been derived from data for 1950–79 (thus being independent from the buoy data annual cycle) and the GCM annual cycle from the 16-year run.

The COADS and buoy data annual cycles show qualitative resemblance but quite large quantitative deviations from each other: Maximum deviations are on the order of 2 m s^{-1}. The buoy zonal winds are mostly stronger than the COADS zonal winds. The buoy meridional winds at 140°W are weaker than in COADS, and in March and April northerly winds are reported from the buoys, while the COADS winds remain southerly. The differences could be due to the limited number of years available for computing mean annual cycles from the buoy data, to the sparsity of ship observations near the buoy sites, and/or to interdecadal wind variations.

The simulated data are of the same order of magnitude as the buoy data but tend to be somewhat weaker. An exception is the zonal wind at 110°W. Here the model simulates stronger than observed winds during February to October. Maximum deviations are on the order of 3 m s^{-1}, which is quite substantial. The annual cycles are similar, but the simulated cycles have minima in February/March, which is one or two months prior to the buoy data's minima in March/April/May.

Comparing the present findings with an earlier evaluation (Biercamp and Storch 1987) of the GCM's wind stress using Han and Lee's (1983) wind stress climatology, we find at 110°W an apparent contradiction: the Han and Lee zonal wind stress is about twice the simulated value, but the zonal GCM wind is in most months larger than the buoy winds. This can be related to two facts, the first being that the meridional wind enters the calculation of the zonal wind stress. At 110°W the model strongly underestimates the meridional wind, which in turn might be related to the model's inability to reproduce an ITCZ of sufficient strength (Kiladis 1988). The second point that may contribute to the bias between the monthly means of simulated stress and surface wind is that the monthly mean of

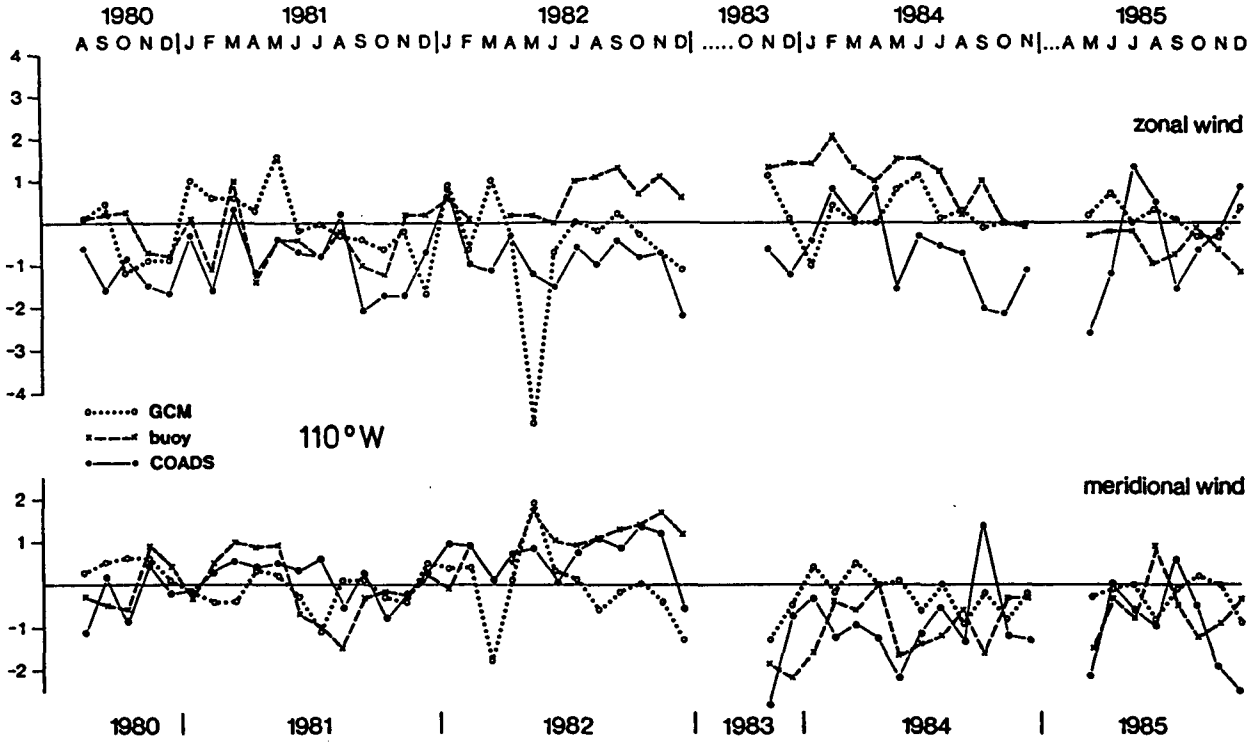

FIG. 3. Time series of anomalous zonal (top) and meridional (bottom) 10 m wind at 110°W as reported from the buoy (crosses) and as simulated by the GCM (open circles). The COADS anomalies taken from a 4° × 10° latitude-longitude grid are added (filled circles). Units: m s^{-1}.

wind stress is composed of mean flow and transient components. The latter are too weakly simulated because the model apparently underestimates the high frequency variability in the eastern tropical Pacific.

c. *Surface winds: anomalies*

The deviations from the annual cycle for the GCM, the buoy, and COADS data at 110°W and at 140°W are shown in Figs. 3 and 4. The COADS zonal wind anomalies at 140°W (Fig. 4) exhibit much more high frequency variance than the buoy data, which is probably related to the particularly poor ship wind data density at this location. From April to June 1985 the COADS zonal wind anomalies seem to be systematically larger (1–3 m s^{-1}) than the buoy data. From October to December 1985 easterly wind anomalies prevailed according to COADS but the buoy data indicated normal conditions at that location. In the case of the 110°W zonal wind anomalies (Fig. 3) a strange pattern of relationships between the buoy and COADS anomalies appears: Until February 1982 the zonal wind anomalies are well correlated, but this is no longer true thereafter. Before February 1982 the mean differences are on the order of 0.5 m s^{-1}, and the anomalies are very close to each other in most cases. After February 1982 typical differences are on the order of 2 m s^{-1},

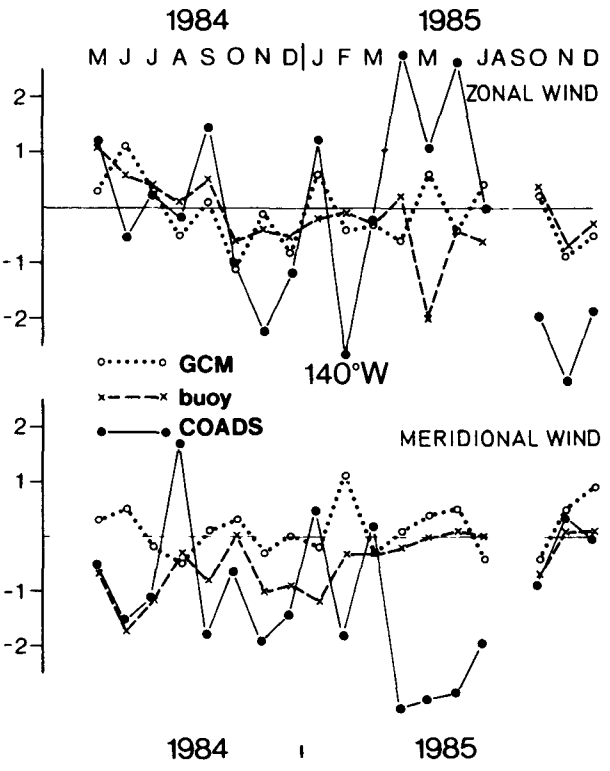

FIG. 4. As in Fig. 3, but at 140°W.

and the signs of the anomalies are for the most part different. Strongest deviations are found in April and May 1982, when the GCM simulates extraordinarily strong negative anomalies.

In particular, it may be inferred from the buoy data that during the entire El Niño event of 1982/83 there were westerly wind anomalies at 110°W, while the COADS data contain easterly zonal wind anomalies until the end of 1982. If, however, the COADS anomalies are calculated using the 1980–86 mean instead of the 1950–79 mean (not shown), the buoy and ship data are in much better agreement. In September 1982, for example, COADS yields anomalies of -0.4 m s^{-1} and 1.1 m s^{-1}, if the 1950–79 and 1980–86 means are used. The latter number compares favorably with the 1.3 m s^{-1} derived from the buoy observations. The FSU data (dataset D), however, indicate easterly zonal stress anomalies for almost the entire year of 1982 and mostly westerly anomalies during 1983.

The low frequency meridional wind anomalies given by the two observed datasets are quite similar, apart from a significant deviation from April to July 1985 at 140°W (Fig. 4).

The comparison of the buoy data and the GCM anomalies leads to the following results: At both 110°W (Fig. 3) and 140°W (Fig. 4), the GCM data are noisier. There is only limited agreement between buoy data and GCM anomalies. On the month-to-month time scale, no similarity exists. On longer time scales there is some coincidence, at least with respect to the general shape of the curves. The model is more successful in simulating the wind anomalies at 140°W than at 110°W. The model fails to reproduce the anomalies observed during the El Niño event of 1982/83. According to the buoy data, this event is accompanied by westerly and northerly wind anomalies of more than 1 m s^{-1}, but in the GCM no persistent anomalies exist.

At 124°W, an annual cycle cannot be derived from the buoy data. Therefore, the full winds are shown in Fig. 5. For comparison, the mean annual cycle as derived from the 1950–79 COADS is added. Based on these annual cycles, the GCM seems to do a fairly good job in reproducing the low frequency changes of the buoy winds. The biggest signal is observed in early 1984 with strong northwesterly anomalies. The GCM qualitatively simulates this feature, but underestimates the zonal wind anomalies significantly.

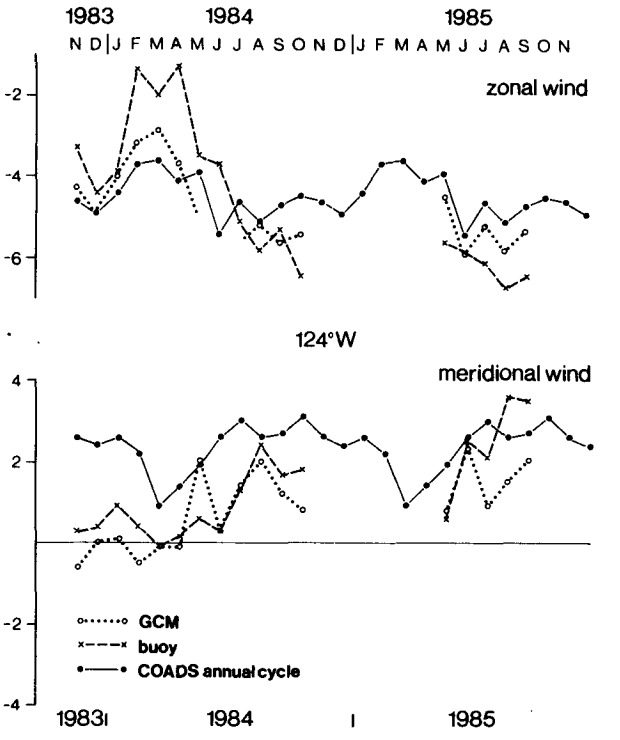

FIG. 5. Time series of zonal (top) and meridional (bottom) 10 m wind at 124°W as reported from the buoy (crosses) and simulated by the GCM (open circles). For comparison the mean annual cycle as derived from the 1950–79 COADS is added (filled circles). Units: m s^{-1}.

d. 850 hPa zonal winds

An inspection of 850 hPa zonal wind anomalies along the equator (not shown) reveals that the phase of observed anomalies (dataset C) is nicely reproduced by our atmospheric GCM. The variability, however, is strongly underestimated with respect to strength and spatial extent. This is substantiated by Fig. 6 showing the standard deviation along the equator in the GCM and in the NMC data. The GCM's variability is markedly confined to the western portion of the tropical Pacific and in general much weaker than in the NMC analyses. The GCM simulates a rather sharp variability maximum near 160°E, while the NMC analyses contain a broad band of high variability between 160°E and 140°W.

e. Surface wind stress

As verification data we use the FSU analyses of surface wind stress (dataset D). We restrict ourselves to the zonal wind stress component, which is the most important forcing function for the equatorial ocean. The annual cycle has been removed and the data have been subjected to low pass filtering retaining variability on time scales greater than 16 months. As was already shown for the 850 hPa zonal winds (Fig. 6) the variability in the model simulation is rather weak. Considering GCM-simulated zonal stress anomalies, the total variance is only about 20% of that derived from the FSU dataset.

EOF analysis of low-pass filtered zonal wind stress anomalies has been carried out for both the FSU dataset and the GCM results. In both cases the first two EOFs, E_1 and E_2, of anomalous zonal wind stress explain

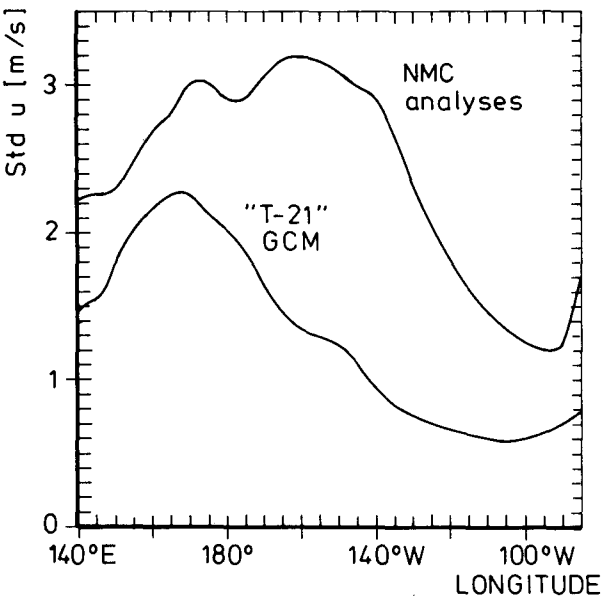

FIG. 6. Standard deviation ($m\ s^{-1}$) of zonal wind anomalies along the equator at the 850 hPa level simulated by the GCM (thin line) and in the NMC analyses (thick line).

more than half of the total variance (observations: 34% and 19%, simulation: 42% and 18%) whereas higher EOFs explain less than one-tenth each.

Both first and second EOFs, as well as their principal components, are shown in Figs. 7 and 8. The spatial characteristics of E_1^{obs} and E_1^{GCM} are quite similar with large positive values over the western tropical Pacific with maximum on the equator near the date line and smaller negative values east of 130°W. The observed tongue of positive values extending from the maximum to the southeast, in the region of the South Pacific Convergence Zone (SPCZ), is not present in the simulation. The patterns of E_2^{obs} and E_2^{GCM} also show some similarities: In both patterns positive values on the equator extend from 150°E to the coast of South America, with positive maxima at about 150°W, 10°S, and negative maxima north of Australia. This region of negative values, however, extends much farther to the east in the observations.

The corresponding first principal components (PC_1) are shown in Fig. 7c. In the time series of PC_1^{obs} all warm and cold phases of the Southern Oscillation can be easily identified, but in the simulated times series PC_1^{GCM} only the strong warm events of 1972/73 and 1982/83, as well as the moderate cold phase prior to 1972, are captured. Cross spectral analysis (not shown) reveals that the two time series are significantly coherent for periods longer than 20 months.

As can be seen from Fig. 8c, the coefficient time series PC_1^{obs} and PC_2^{obs} of the first and second observed EOF vary over most of the 16-year period quite coherently with a phase shift of one-half to one year. This may be interpreted as a "cyclic mode" with E_1^{obs} (Fig. 7a) being the characteristic anomaly at the time of an El Niño (or a La Niña) event and E_2^{obs} (Fig. 8a) describing an eastward shift during the transition phase between these events. An eastward propagation of zonal surface wind anomalies was also found by Barnett (1983) using the technique of complex EOFs.

The cyclic behavior of the first two observed EOFs is especially clear during the period of 1982–83. In March/April 1982 PC_2^{obs} has a minimum and, at the same time, PC_1^{obs} is almost zero. Thus the sum of the two contributions to the full signal reduces to $-E_2^{obs}$ with a large amplitude, i.e., during the onset stage of the 1982/83 El Niño the observations show strong easterly wind stress anomalies between 5°N and 20°S and westerly anomalies south of 20°S and over most of the northern part of the basin.

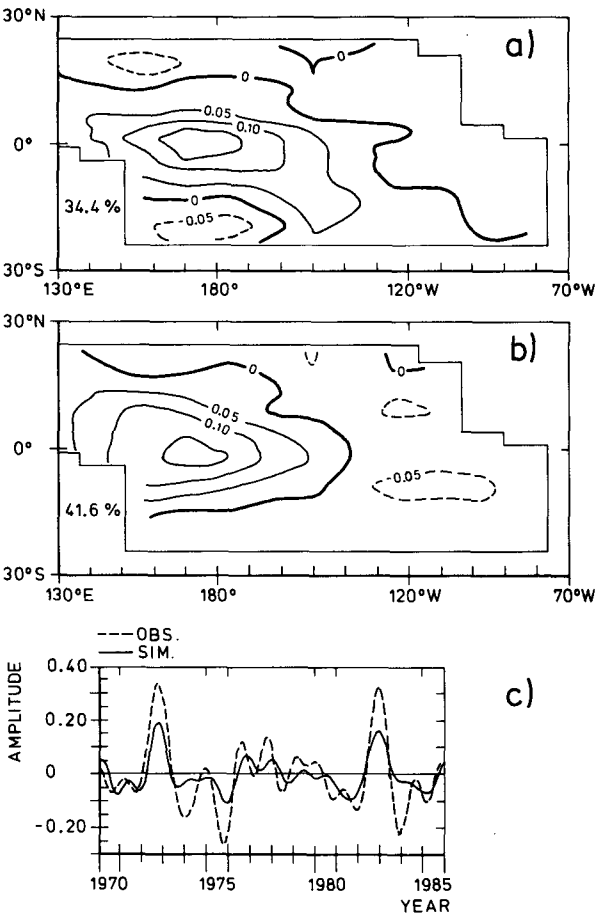

FIG. 7. First Empirical Orthogonal Functions (EOFs) of low-pass filtered (periods greater than 16 months retained) zonal wind stress anomalies derived from 1961–85 FSU analyses (a) and from the GCM experiment (b). The explained variance is 34.4% for the observations and 41.6% for the simulation. The corresponding coefficient time series are shown in (c). Dashed line: FSU analyses. Solid line: GCM.

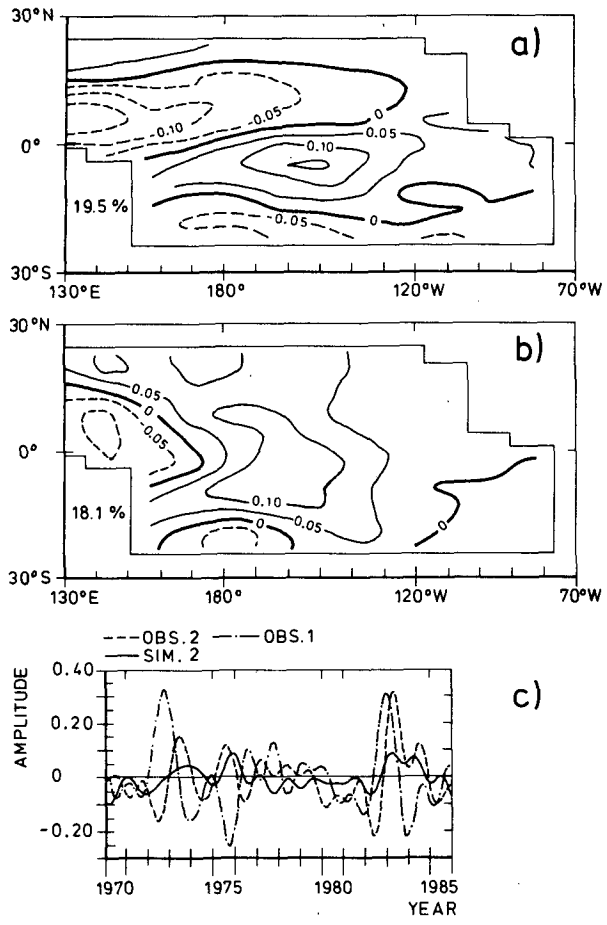

FIG. 8. As in Fig. 7 but for the second EOFs. Explained variances are 19.5% (observations: solid line) and 18.1% (simulation: dashed line). For reference, the coefficient time series of the first EOF derived from the FSU dataset is added in (c) as dash-dotted line.

At the end of 1982 when the event is fully developed with large SST anomalies in the eastern equatorial Pacific (not shown), the wind stress anomalies are dominated by E_1^{obs}, i.e., by large westerly anomalies over the western and central equatorial Pacific. In April/May 1983 the pattern E_2^{obs} dominates so that westerly anomalies have moved to the east and are now centered at 150°W extending from Australia to the Peruvian coast. At the end of 1983 E_1^{obs} is again dominant but with reversed sign: Over the easternmost part of the Pacific small westerly anomalies remain, but over the western and central Pacific wind stress anomalies now have a large easterly component.

Comparing the coefficient time series PC_1^{GCM} and PC_2^{GCM} derived from the GCM results, no coherent phase relationship appears (Figs. 7c and 8c); i.e., the first two simulated EOFs, E_1^{GCM} and E_2^{GCM}, do not describe a cyclic sequence of propagating patterns. There may be two reasons for this: There is no pattern in the GCM data playing the role of E_2^{obs}, or this pattern is described by higher indexed EOFs or by a linear combination of EOFs. We will see later that the former explanation is correct.

4. Sensitivity of SST to wind stress differences

The EOF analysis of simulated and observed zonal wind stresses leads us to the following two hypotheses:

(i) The part of the observed wind stress variability that is related to low-frequency variations of SST is mainly described by the first two EOFs E_1^{obs} and E_2^{obs}.

(ii) The simulated wind stress field is insufficient to reproduce the complete observed sequence of El Niño and La Niña events, if it is used to drive an ocean model.

To assess the validity of these hypotheses an equatorial oceanic GCM, used in previous coupled ocean–atmosphere simulations (Latif et al. 1988a,b), has been driven with various forcing fields for the period 1970 to 1985:

1) The full observed wind stress forcing derived from FSU analyses;
2) the observed forcing, low-pass filtered and truncated to the first EOF shown in Fig. 7a;
3) the observed forcing, low-pass filtered and truncated to the first two EOFs shown in Figs. 7a and 8a;
4) the full simulated wind stress forcing; and
5) the low-pass filtered simulated forcing truncated to the first EOF shown in Fig. 7b.

The experiments have been carried out by spinning up the ocean model with the observed (simulated) annual mean surface wind stress for 1 year and with the observed (simulated) climatological annual cycle for 4 years. Thereafter the different anomalous forcing fields have been added to the climatological annual cycle during the above described 16-year integrations.

The results obtained in experiment 1) have been presented in detail by Latif (1987), who compared the simulated SST with observed SST. He found that low frequency variations of SST are reproduced by the model in the western Pacific. In the eastern Pacific the results are less consistent, but at least the major El Niño episodes (1972/73 and 1982/83) are reproduced.

In this section and section 5, we use the results of experiment 1) as a reference against which to compare the SST obtained in the other experiments. The results are shown as time series of simulated SST anomalies at two equatorial locations: One at the date line (Fig. 9) and the other in the eastern Pacific at 110°W (Fig. 10). The SST simulated in 4) and 5) were almost identical. Therefore, simulation 5) is not shown.

If we truncate the observed wind stress fields to the first EOF only [experiment 2)], the low frequency variability of SST at both locations is significantly

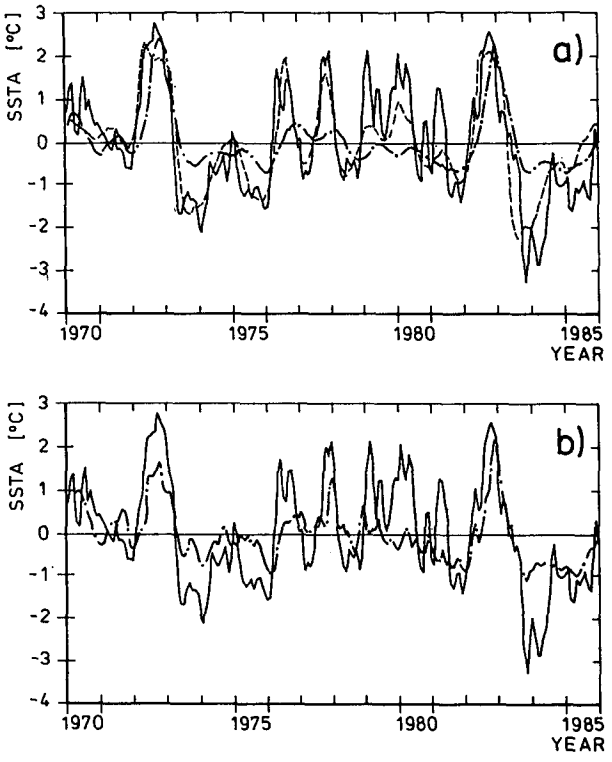

FIG. 9. SST response of the OGCM on the equator at the date line to (a) observed and (b) simulated wind stress. The solid lines show the SST anomalies which are obtained in the reference experiment 1) when the ocean model is forced with the FSU analyses. (a) Dash-dotted line is the response to the observed forcing which has been truncated to the first EOF [experiment 2)]; dashed line; response to observed forcing truncated to the first two EOFs [experiment 3)]. (b) Dashed-dotted line is the response to the full simulated forcing [experiment 4)].

weaker than in the reference run [experiment 1)]. At the date line (Fig. 9a) this reduction is most pronounced during the major cold events of 1973, 1975, and during the minor cold event of 1983/84. The two major warm events of 1972/73 and 1982/83 are well simulated at this location. In the eastern Pacific (Fig. 10a) low frequency variability is weak throughout the entire 16-year period. This result is a reflection of the spatial pattern of the first EOF (Fig. 7a), which has no significant contribution over the eastern Pacific.

In experiment 3) simulated SST anomalies at the date line (Fig. 9a) become very close to the anomalies obtained in the reference run with full wind stress forcing. This is best seen for the three cold phases mentioned above. The simulation of eastern Pacific SST anomalies is also improved when the second EOF is added (Fig. 10a). At this location, however, there still remain serious differences from the reference run: First, a phase shift of a few months for the onset of the warm event of 1972/73, and second, a strongly reduced amplitude during the later stages of the 1982/83 warm event. Nevertheless, we conclude from the OGCM experiments 2) and 3) that most of the low frequency SST variability can be accounted for if only the first two EOFs are retained in the wind stress field. Thus, we accept our hypothesis (i).

The SST anomalies obtained when the ocean model is forced with the full GCM-simulated wind stress [experiment 4)] are shown in Figs. 9b and 10b. Consistent with our earlier results for the wind stress, the variance of SST is considerably reduced compared to the reference run. The ENSO signal in the western Pacific is, apart from the two warm events of 1972/73 and 1982/83, much too weak. In the eastern Pacific it is virtually absent, so that only the two aforementioned warm events can be detected with severely underestimated amplitude. Thus, hypothesis (ii) turns out to be correct also.

More important than the general underestimation of SST variance, however, is the similarity of the results obtained in experiment 4) with those from experiments 2) and 5), when only the first "observed" or "simulated" EOF was used as the anomalous forcing. From this similarity we infer that nothing in the simulated wind field plays the role of the second "observed" EOF, and that the ENSO-related SST signal in the "simulated forcing runs" is already obtained if the ocean model is driven by the first "simulated" EOF only.

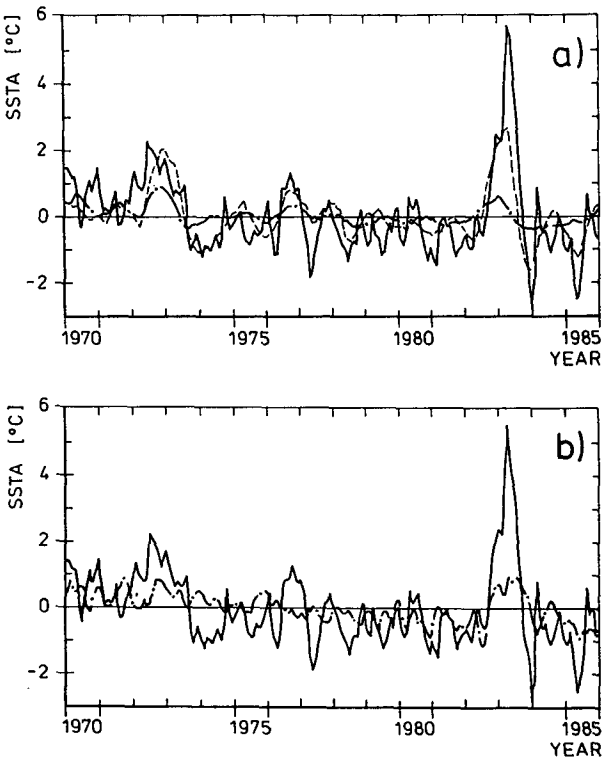

FIG. 10. As in Fig. 9, but at 110°W.

5. Statistical a posteriori improvement of simulated wind stress

The results for the AGCM response found in section 4 are disappointing, because they indicate that the atmospheric GCM in its present form is not well suited to represent the atmospheric part of a coupled ocean–atmosphere model. A possibility for overcoming the shortcomings in the simulated wind stress, at least for ENSO prediction studies with our coupled model, may be the application of Model Output Statistics (MOS), a method which is routinely used in operational weather forecasting (Glahn and Lowry 1972). In this paper we use the technique as a diagnostic tool to find out how the simulated wind stress anomalies may be changed to give a better ocean response.

If the observations at a certain time t are represented by an $\mathcal{M}$-dimensional vector $\mathbf{q}(t)$ and the simulated data by an $\mathcal{N}$-dimensional vector $\mathbf{p}(t)$, we are looking for a $\mathcal{M} \times \mathcal{N}$ matrix $\mathfrak{L}$ minimizing

$$\langle \| \mathfrak{L}\mathbf{p}(t) - \mathbf{q}(t) \|^2 \rangle \qquad (1)$$

where $\| \cdot \|$ is the Euclidean vector norm and $\langle \cdot \rangle$ denotes expectation. $\mathfrak{L}$ is a linear operator that tells us how the simulated data, p^1 to $p^{\mathcal{N}}$, must be changed to give on average an optimal representation of the observations, q^1 to $q^{\mathcal{M}}$. Note that neither the number nor the physical parameter represented by the vectors $\mathbf{q}$ and $\mathbf{p}$ need be the same. For instance, $\mathbf{q}$ might represent 850 hPa zonal wind on a fine grid and $\mathbf{p}$ surface wind stress on a coarse grid. The solution of (1) is given by

$$\mathfrak{L} = \langle \mathbf{q}(t)\mathbf{p}(t) \rangle \cdot \langle \mathbf{p}(t)\mathbf{p}(t) \rangle^{-1}. \qquad (2)$$

In our case, we use $\mathbf{q}$ = FSU analyses of zonal wind stress and $\mathbf{p}$ = GCM simulated wind stress, both interpolated onto the grid of the ocean model. We consider different choices for designing the MOS approach:

1) $\mathbf{q}$ and $\mathbf{p}$ represent the grid-point data covering the whole tropical Pacific with $\mathcal{N} = \mathcal{M} = 650$.

2) Equation (1) is solved at each grid point separately, i.e. $\mathcal{N} = \mathcal{M} = 1$, with $\mathbf{q}$ and $\mathbf{p}$ observed and simulated wind stress at location j, respectively.

3) $\mathbf{q}$ and $\mathbf{p}$ are composed of EOF coefficients PC_j^{obs} and PC_j^{GCM}.

Approach 1) is impractical, because with the presently available data we cannot derive a reliable estimate of $\mathfrak{L}$ by means of (2), which requires the dimensions $\mathcal{N}$ and $\mathcal{M}$ to be significantly smaller than the sample size. In our case the latter number is $16 \times 12 = 192$ (number of years $\times$ 12 months). We call 2) LOS (Local Output Statistics) and 3) POS (Pattern Output Statistics).

After having determined the "correction matrix" $\mathfrak{L}$, the GCM generated wind stress anomalies can be corrected interactively in the coupled atmosphere–ocean system. In the present paper we investigate the possible merits of the MOS technique by forcing the ocean GCM with a posteriori corrected wind stress, i.e., by $\mathfrak{L}p$ instead by p. The results of the correction are time series of zonal wind stress anomalies, whose statistics are determined from the observations, while their time evolution is computed by the AGCM.

The results of the LOS approach 2) and of the POS approach 3) are presented by showing the ocean GCM's response to the LOS and POS corrected GCM wind stress anomalies at the two equatorial locations already used in section 4, namely, 180° and 110°W (Fig. 11).

a. Results obtained with LOS

For the LOS approach 2) the matrix $\mathfrak{L}$ reduces to a single number estimated for each grid point separately. In our case, $\mathfrak{L}$ varies between 1 and 2.5 over most of the equatorial Pacific.

Using LOS-corrected GCM wind stress anomalies leads to a SST simulation that is very similar to that making use of POS corrected wind stress. Therefore, the LOS SST time series at the two equatorial locations are not shown. The results are discussed together with the "POS-results" in section 5b.

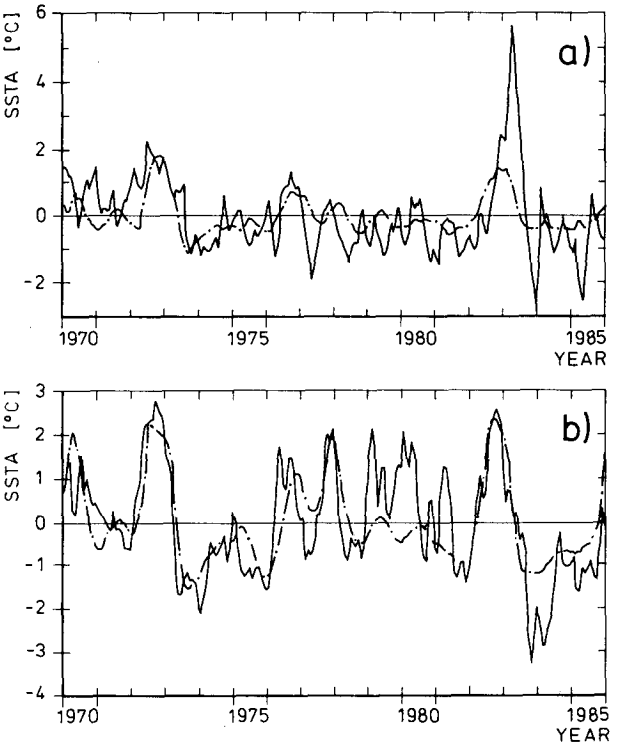

FIG. 11. SST response of the OGCM on the equator at 110°W (a) and at the date line (b) to POS-corrected simulated wind stress. The solid lines show the SST anomalies which are obtained in the reference experiment 1), when the ocean model is forced with the FSU analyses. Dash–dotted lines are the response to POS-corrected wind stress.

b. Results obtained with POS

For the POS approach 3) we use the two first principal components of low-pass filtered wind stress, i.e., $\mathcal{N} = \mathcal{M} = 2$, $\mathbf{q} = (PC_1^{obs}, PC_2^{obs})^T$ and $\mathbf{p} = (PC_1^{GCM}, PC_2^{GCM})^T$. The correction matrix $\mathfrak{L}$ derived from (2) is

$$\mathfrak{L} = \begin{pmatrix} 1.71 & 0.53 \\ -0.23 & 1.40 \end{pmatrix}.$$

This matrix describes an enhancement of the simulated principal components in the main diagonal (the elements are larger than 1) and a slight mixture of the two EOF coefficients.

The a posteriori correction of wind stress anomalies for use in the ocean GCM is given by

$$\tau^* = \tau + [(E_1^{obs}, E_2^{obs}) \cdot \mathfrak{L} - (E_1^{GCM}, E_2^{GCM})] \begin{pmatrix} PC_1^{GCM} \\ PC_2^{GCM} \end{pmatrix} \quad (3)$$

where τ denotes the "raw" GCM simulated and τ^* the corrected anomalous wind stress. Note that the POS approach (C) changes not only the variance but also the patterns by replacing the simulated EOF patterns by the observed EOF patterns.

POS and LOS both lead to an obvious improvement of the SST simulation on the ENSO time scale at the date line (Fig. 11b), which is best seen for the two cold events of 1973 and 1975. Large deviations from the reference run are still found for the strong cooling following the 1982/83 event and the large positive anomalies during 1979 and 1980 in the western Pacific. Interestingly, both of these features are not found in certain observations. Hence one might speculate that by combining the information about the dominant modes from the FSU analyses and the GCM output, we can improve the forcing fields in some aspects. At the eastern equatorial Pacific location, LOS and POS lead to a moderate improvement (Fig. 11a). The large positive SST anomalies (up to almost 6°C) during the 1982/83 El Niño cannot be entirely simulated, because LOS and POS cannot account for extraordinary events, if the simulation is not extraordinary itself.

Using larger numbers for $\mathcal{N}$ and $\mathcal{M}$ did not improve our results significantly. On the other hand it is not sufficient to use the first EOF only, which can be deduced from hypothesis (i) presented in section 4.

6. Summary and discussion

The tropical near-surface response of the T21 model to globally varying observed SST from 1970 to 1985 was compared to observations. The comparison is more favorable for the largest scales and for time periods longer than one year than it is for local data and shorter time scales.

There is a Southern Oscillation induced by the time-dependent SST in our atmospheric GCM (Fig. 1), which is not found in a control run with climatologically varying SST.

Considering surface wind at selected equatorial locations, no similarities between simulated and observed data were found on the month to month time scale. Agreement on the ENSO time scale with the observed time series is difficult to discern because buoy time series are too short and COADS anomalies are too noisy (Figs. 3, 4, and 5).

Low frequency changes of the simulated Southern Oscillation are correct in phase but mainly restricted to the western and central equatorial Pacific, which are key areas for large scale air–sea interactions, whereas they are hardly detectable over the eastern equatorial Pacific (Fig. 6). The variance of the low frequency changes is strongly reduced in our model simulation (Figs. 6 and 7c).

With respect to single events the model is fairly successful in reproducing the warm events in 1972/73 and 1982/83 and the cold event in 1970/71. The cold events of 1973/74 and 1975/76 and the moderate warm phases of 1976 and 1977, on the other hand, can be identified in the simulations but are much less pronounced than observed.

At higher frequencies, observed and simulated changes are uncorrelated, but the variances over the eastern Pacific are comparable, as could be inferred from the comparison of simulated surface wind anomalies with those reported by the buoys (Fig. 3).

An EOF analysis of the observed zonal wind stress reveals that the Southern Oscillation may be approximated by an eastward migrating pattern centered on the equator. That is, the Southern Oscillation may be formally written as a stochastic cyclic sequence of patterns:

$$\cdots \rightarrow E_1^{obs} \rightarrow E_2^{obs} \rightarrow -E_1^{obs} \rightarrow -E_2^{obs} \rightarrow E_1^{obs} \rightarrow E_2^{obs} \rightarrow \cdots.$$

The characteristic numbers are: zonal length scale, 8000 km; meridional length scale, 4000 km; time scale, 2 years.

The simulated wind stress, on the other hand, may conveniently be described by just one EOF, as has been demonstrated by the OGCM experiments. That is, the simulated zonal wind stress anomalies have a dominant standing mode of low frequency variability and can therefore be described by the leading low frequency EOF only (Fig. 7):

$$\cdots \rightarrow E_1^{GCM} \rightarrow -E_1^{GCM} \rightarrow E_1^{GCM} \rightarrow -E_1^{GCM} \rightarrow \cdots.$$

We conclude that the AGCM in its present version suffers from two major model flaws limiting its value

in simulating tropical atmosphere–ocean interaction. First, while the pattern of the first zonal wind stress EOF compares favorably with observations (Figs. 7a and 7b), the corresponding principal components (Fig. 7c) reveal a significant underestimation of the strength of the simulated anomalies. Second, the AGCM does not simulate the eastward migration of these anomalies, which could be inferred from the fact that its first two EOFs are not in quadrature to each other, as is the case for the observations (Fig. 8). These deficiencies consequently lead to weak interannual variability which is particularly marked over the eastern Pacific.

The underestimation of the strength of stress anomalies over the western Pacific is probably closely related to the failure of the AGCM to simulate a realistic climate mean state, which is exemplified by much too weak trade winds over the Pacific (Biercamp and Storch 1987). Both errors might be related to the parameterization of deep convection, which presumably is not adequately tuned for our purposes, resulting in a weak sensitivity of the large scale tropical circulation to changes in SST.

It is not yet clear why the AGCM fails to simulate the observed eastward migration of anomalies, since it is commonly accepted that (at least for the 1982/83 El Niño) the propagation of atmospheric anomalies was caused by the eastward migration of warm water across the Pacific (Gill and Rasmusson 1983). This is further supported by the model study of Fennessy and Shukla (1988), who performed a more realistic simulation of this particular event by prescribing the observed SST. It is interesting that the AGCM developed at GFDL shows a similar result to ours. As described by Barnett (1985) the Southern Oscillation in this model also appears as a standing feature. All of the described models make use of different convection schemes, so that one can only speculate that the scheme used in the model by Fennessy and Shukla (1988) might be more suitable for our purposes than the other two schemes.

Another possible reason why our AGCM failed may be the choice of the SST climatology (Alexander and Mobley 1976), which exhibits systematically lower temperatures in the eastern Pacific than other climatologies (e.g., Reynolds 1988). Because we added observed SST anomalies to the climatology of Alexander and Mobley (1976), temperatures of 29°C or more are hardly reached during the integration. The underestimation of tropical SST might limit deep convection in some areas and even preclude it at other locations. That is, the energy transfer might simply be cut off as the warm water moves eastward. Notice that the observations indicate the existence of 29°C water in the eastern Pacific in boreal spring 1983 for several months (Gill and Rasmusson 1983) and that in the model study of Fennessy and Shukla (1988) SST also reached similar values in the east.

A major goal of this paper is to gain insight into the dynamics of our coupled ocean–atmosphere model (Latif et al. 1988a,b), which does not show low frequency oscillations in a 10-year integration. Our analyses of AGCM-simulated surface wind stress anomalies support the speculation of Latif et al. (1988b) that the weak interannual variability in our coupled model may partly be attributed to the AGCM. Certainly, other problems in the coupled system can be attributed to the OGCM and to the coupling technique applied.

Because the results of the AGCM simulation are highly coherent with observations, however, the application of a MOS-technique may help to overcome some of these problems. We have shown that the simulation of SST anomalies can be significantly improved if MOS-corrected wind stress anomalies are used as anomalous forcing (Fig. 11). This multiplicative correction scheme is presently being tested in ENSO hindcast experiments with our coupled model. Such a correction, however, could only be an intermediate solution until our AGCM has been improved to give a more realistic response to anomalous SST.

Acknowledgments. We thank Phil Arkin for the NMC data and Marion Grunert, who thoroughly prepared the diagrams. We also wish to express our gratitude to the Director of the Max Planck Institut für Meteorologie, Klaus Hasselmann, for encouraging and supporting us. The work was in part financed by the European Community/Natural Hazards program under Grant EV4C-0035-D(B) and by NOAA's Equatorial Pacific Ocean Climate Studies (EPOCS) Program, Pacific Marine Environmental Laboratory Contribution number 1148.

REFERENCES

Alexander, R. C., and R. L. Mobley, 1976: Monthly average sea surface temperature and ice pack limits for 1 deg global grid. *Mon. Wea. Rev.*, **104**, 143–148.

Arkin, P. A., 1982: The relationship between interannual variability in the 200 hPa tropical wind field and the Southern Oscillation. *Mon. Wea. Rev.*, **110**, 1393–1404.

Barnett, T. P., 1983: Interaction of the monsoon and the Pacific trade wind system at interannual time scales. Part I: The equatorial zone. *Mon. Wea. Rev.*, **111**, 756–773.

——, 1985: Variations in near-global sea level pressure. *J. Atmos. Sci.*, **42**, 478–501.

Biercamp, J., and H. v. Storch, 1987: Exchange of energy and momentum at the ocean's surface. Climate simulations with the ECMWF T21 model in Hamburg, Large Scale Atmospheric Modelling Report 1, 1986, G. Fischer, Ed., Meteorologisches Institut der Universität Hamburg, Bundesstr. 55, D2000 Hamburg 13, Federal Republic of Germany, 83–94.

Chervin, R. M., 1988: Predictability of time-averaged atmospheric states. *Physically-Based Modelling and Simulation of Climate and Climate Change—Part II*, M. E. Schlesinger, Ed., Kluwer Academic Publishers, 983–1008.

Dümenil, L., and U. Schlese, 1987: Description of the General Circulation model. Climate simulations with the ECMWF T21 model in Hamburg, Large Scale Atmospheric Modelling Report

1, G. Fischer, Ed., Meteorologisches Institut der Universität Hamburg, Bundesstr. 55, 2000 Hamburg 13, Federal Republic of Germany, 3–10.

Fennessy, M. J., and J. Shukla, 1988: Numerical simulation of the atmospheric response to the time-varying El Niño SST anomalies during May 1982 through October 1983. *J. Climate,* **1,** 195–211.

Fischer, G., 1987: Climate simulations with the ECMWF T21 model in Hamburg. Large Scale Atmospheric Modelling Report 1, G. Fischer, Ed., Meteorologisches Institut der Universität Hamburg, Bundesstr. 55, 2000 Hamburg 13, Federal Republic of Germany, 3–10.

Freitag, H. P., M. J. McPhaden and A. J. Shepherd, 1989: Comparison of equatorial winds as measured by cup vs propeller anemometers. *J. Atmos. Oceanic Technol.,* **6,** 327–332.

Gill, A. E., and E. M. Rasmusson, 1983: The 1982–83 climate anomaly in the equatorial Pacific. *Nature,* **306,** 229–234.

Glahn, H. R., and D. A. Lowry, 1972: The use of model output statistics (MOS) in weather forecasting. *J. Appl. Meteor.,* **11,** 1203–1211.

Goldenberg, S. B., and J. J. O'Brien, 1981: Time and space variability of tropical Pacific wind stress. *Mon. Wea. Rev.,* **109,** 1190–1207.

Graham, N. E., T. P. Barnett, R. M. Chervin, M. E. Schlesinger and U. Schlese, 1988: Comparisons of GCM and observed surface wind fields over the tropical Indian and Pacific oceans. *J. Atmos. Sci.,* **46,** 760–788.

Han, Y. J., and S. W. Lee, 1983: A new analysis of monthly mean wind stress over the global ocean. *Mon. Wea. Rev.,* **111,** 1554–1566.

Kiladis, G., 1988: Some comments on the T21 model's precipitation climatology. Climate simulations with the ECMWF T21 model in Hamburg, Large Scale Atmospheric Modelling Report 4, H. von Storch, Ed., Meteorologisches Institut der Universität Hamburg, Bundesstr. 55, 2000 Hamburg 13, Federal Republic of Germany, 3–10.

Kirk, E., M. Ponater and A. Kirk, 1987: Circulation statistics of T21 GCM. Climate simulations with the ECMWF T21 model in Hamburg. Large Scale Atmospheric Modelling Report 1, 1986, G. Fischer Ed., Meteorologisches Institut der Universität Hamburg, Bundesstr. 55, 2000 Hamburg 13, Federal Republic of Germany, 11–30.

Large, W. G., and S. Pond, 1981: Open ocean momentum flux measurements in moderate to strong winds. *J. Phys. Oceanogr.,* **11,** 324–336.

Latif, M., 1987: Tropical ocean circulation experiments. *J. Phys. Oceanogr.,* **17,** 246–263.

——, J. Biercamp and H. v. Storch, 1988a: The response of a coupled ocean-atmosphere general circulation model to wind bursts. *J. Atmos. Sci.,* **45,** 964–979.

——, ——, —— and F. J. Zwiers, 1988b: A ten year climate simulation with a coupled ocean-atmosphere general circulation model. MPI-Report No. 21, Max-Planck-Institut für Meteorologie, Bundesstr. 55, D-2000 Hamburg 13, Federal Republic of Germany.

Lau, N.-C., 1985: Modeling the seasonal dependence of the atmospheric response to observed El Niños in 1962–76. *Mon. Wea. Rev.,* **113,** 1970–1996.

Leetmaa, A., and M. Ji, 1989: Operational hindcasting of the tropical Pacific. *Dyn. Atmos. Oceans,* **13,** 465–490.

Legler, D. M., and J. J. O'Brien, 1984: Atlas of tropical Pacific wind stress climatology 1971–1980. Florida State University, Department of Meteorology, Tallahassee FL 32306, 182 pp.

McPhaden, M., and B. A. Taft, 1988: On the dynamics of seasonal and intraseasonal variability in the eastern equatorial Pacific. *J. Phys. Oceanogr.,* **18,** 1713–1732.

Reynolds, R. W., 1988: A real-time global sea surface temperature analysis. *J. Climate,* **1,** 75–86.

Storch, H. v., 1988: Climate simulations with the ECMWF T21 model in Hamburg. Large Scale Atmospheric Modelling Report 4, H. von Storch, Ed., Meteorologisches Institut der Universität Hamburg, Bundesstr. 55, 2000 Hamburg 13, Federal Republic of Germany, 3–10.

Trenberth, K. E., and J. G. Olson, 1988: Evaluation of NMC global analyses: 1979–1987. NCAR Technical Note NCAR/TN-299+STR. National Center for Atmospheric Research, Boulder, Colorado.

Wallace, J. M., and Q. Jiang, 1987: On the observed structure of the interannual variability of the atmosphere/ocean climate system. *Atmospheric and Oceanic Variability,* H. Cattle, Ed., Royal Meteor. Soc., Bracknell, Berkshire, United Kingdom, 182 pp.

Wright, P. B., 1988: At atlas based on the 'COADS' data set: Fields of mean wind, cloudiness and humidity at the surface of the global ocean. MPI-Report No. 14, Max-Planck-Institut für Meteorologie, Bundesstrasse 55, D-2000 Hamburg 13, Federal Republic of Germany.

Wyrtki, K., 1975: El Niño—The dynamical response of the equatorial Pacific ocean to atmospheric forcing. *J. Phys. Oceanogr.,* **5,** 572–584.